Naval Research Laboratory
Washington, DC 20375-5320

NRL/8230/MR—2023/2

Applications of Sliding Mode Control to Orbital Rendezvous with Tumbling or Maneuvering Clients

BRYAN PATRIC HOSKINS

Dynamics and Control Systems Branch
Spacecraft Engineering Division

November 13, 2023

REPORT DOCUMENTATION PAGE

Form Approved
OMB No. 0704-0188

1. REPORT DATE *(DD-MM-YYYY)*	**2. REPORT TYPE**	**3. DATES COVERED** *(From - To)*
13-11-2023	NRL Memorandum Report	08/03/2021 - 08/01/2023

4. TITLE AND SUBTITLE

Applications of Sliding Mode Control to Orbital Rendezvous with Tumbling or Maneuvering Clients

5a. CONTRACT NUMBER

5b. GRANT NUMBER

5c. PROGRAM ELEMENT NUMBER
NISE

6. AUTHOR(S)

Bryan Patric Hoskins

5d. PROJECT NUMBER

5e. TASK NUMBER

5f. WORK UNIT NUMBER
N20N

7. PERFORMING ORGANIZATION NAME(S) AND ADDRESS(ES)

Naval Research Laboratory
4555 Overlook Avenue, SW
Washington, DC 20375-5320

8. PERFORMING ORGANIZATION REPORT NUMBER

NRL/8230/MR--2023/2

9. SPONSORING / MONITORING AGENCY NAME(S) AND ADDRESS(ES)

Naval Research Laboratory
4555 Overlook Avenue, SW
Washington, DC 20375-5320

10. SPONSOR / MONITOR'S ACRONYM(S)

NRL-NISE

11. SPONSOR / MONITOR'S REPORT NUMBER(S)

12. DISTRIBUTION / AVAILABILITY STATEMENT

DISTRIBUTION STATEMENT A: Approved for public release; distribution is unlimited.

13. SUPPLEMENTARY NOTES

Karles Fellowship

14. ABSTRACT

The capabilities of autonomous inspection vehicles that operate near malfunctioning clients have developed significantly over the last decade due to their rapidly evolving mission set. On-orbit inspection serves as a necessary catalyst to gain vital information of a prospective client vehicle prior to executing a servicing operation. The associated challenges are augmented when the client is deemed inoperable or malfunctioning, such that the inspector is incapable of actively assisting in a coordinated rendezvous maneuver. The nature of a client, deemed either inoperable or malfunctioning, suggest that the client could be uncontrollably tumbling, or translationally maneuvering, due to a damaged propulsion system. Therefore, the focus of this study is to investigate the satellite relative position control problem, which enables an autonomous inspection vehicle to approach, and operate around, a malfunctioning client capable of producing uncertain maneuvering. The line-of-sight based relative motion model is first introduced, being formulated in a coordinate frame attached to the inspector, not client, which leverages the navigation information directly. The state of the client could be partially or completely unknown, and therefore, it's more convenient to formulate the dynamic model in a frame attached to the inspecting vehicle. This investigation then synthesizes adaptive and robust control into a single, continuous framework without bounding knowledge of unknown perturbation and uncertainties in the form of an adaptive second-order fast non-singular terminal sliding mode control law. The proposed control scheme is designed to deliver an inspection vehicle into proximity of a freely tumbling, or maneuvering client, while ensuring finite-time convergence of the sliding variables to the design manifold, in spite of these system uncertainties and perturbations. The proposed control scheme is then proven stable in the Lyapunov regime, achieving convergence when the upper bounds of the bounded uncertainties are unknown a priori. Finally, several numerical simulations are presented to demonstrate the effectiveness of the proposed adaptive second-order fast non-singular terminal sliding mode controller and its application to future on-orbit inspection missions with malfunctioning or inoperable clients.

15. SUBJECT TERMS

Adaptive control; Sliding mode control; Terminal sliding mode control; Second-order terminal sliding mode control; Adaptive second-order fast non-singular Terminal sliding mode control; Spacecraft position control; Tumbling; Uncertain maneuver; Autonomous RPO; Nonlinear spacecraft dynamics

16. SECURITY CLASSIFICATION OF:			**17. LIMITATION OF ABSTRACT**	**18. NUMBER OF PAGES**	**19a. NAME OF RESPONSIBLE PERSON**
					Bryan P. Hoskins
a. REPORT	**b. ABSTRACT**	**c. THIS PAGE**	U	21	**19b. TELEPHONE NUMBER** *(include area code)*
U	U	U			(202) 404-4374

This page intentionally left blank.

APPLICATIONS OF SLIDING MODE CONTROL TO ORBITAL RENDEZVOUS WITH TUMBLING OR MANEUVERING CLIENTS

Bryan P. Hoskins*

The capabilities of autonomous inspection vehicles that operate near malfunctioning clients have developed significantly over the last decade due to their rapidly evolving mission set. On-orbit inspection serves as a necessary catalyst to gain vital information of a prospective client vehicle prior to executing a servicing operation. The associated challenges are augmented when the client is deemed inoperable or malfunctioning, such that the inspector is incapable of actively assisting in a coordinated rendezvous maneuver. The nature of a client, deemed either inoperable or malfunctioning, suggest that the client could be uncontrollably tumbling, or translationally maneuvering, due to a damaged propulsion system. Therefore, the focus of this study is to investigate the satellite relative position control problem, which enables an autonomous inspection vehicle to approach, and operate around, a malfunctioning client capable of producing uncertain maneuvering. The line-of-sight based relative motion model is first introduced, being formulated in a coordinate frame attached to the inspector, not client, which leverages the navigation information directly. The state of the client could be partially or completely unknown, and therefore, it's more convenient to formulate the dynamic model in a frame attached to the inspecting vehicle. This investigation then synthesizes adaptive and robust control into a single, continuous framework without bounding knowledge of unknown perturbation and uncertainties in the form of an adaptive second-order fast non-singular terminal sliding mode control law. The proposed control scheme is designed to deliver an inspection vehicle into proximity of a freely tumbling, or maneuvering client, while ensuring finite-time convergence of the sliding variables to the design manifold, in spite of these system uncertainties and perturbations. The proposed control scheme is then proven stable in the Lyapunov regime, achieving convergence when the upper bounds of the bounded uncertainties are unknown *a priori*. Finally, several numerical simulations are presented to demonstrate the effectiveness of the proposed adaptive second-order fast non-singular terminal sliding mode controller and its application to future on-orbit inspection missions with malfunctioning or inoperable clients.

INTRODUCTION

With an increased dependency on the space domain, the number of spacecraft deemed inoperable or malfunctioning will undoubtedly increase, leading to new operational requirements for more complex inspection and servicing sorties. Satisfying these mission requirements will be vital to the future of spaceflight, as maneuvering to inoperable or malfunctioning client vehicles unprepared for on-orbit servicing presents unique challenges to operating servicing vehicles. These challenges manifest from the assumption that the client is unprepared for on-obit servicing, and therefore, incapable of actively assisting in a coordinated maneuver. Spacecraft are designed to be lightweight and are often built without considerations for future maintenance, and therefore would be lacking the necessary hard points to facilitate on-orbit servicing subsequent to an operational anomaly resulting in a damaged asset, rendering it malfunctioning or entirely inoperable. Moreover, potentially damaged assets could feasibly exhibit uncertain, and therefore hazardous behaviors such as uncontrolled tumbling or translational maneuvering.

The unprepared nature of the client coupled with its uncertain behavior prompts a need for on-orbit inspection prior to any servicing operations. However, the area of research related to autonomous operations

*Aerospace Engineer, U.S. Naval Research Laboratory, 4555 Overlook Ave SW, Washington, D.C. 20375

Manuscript approved October 13, 2023.

with malfunctioning clients is still facing many technical challenges which include dynamic modeling, guidance, navigation and control, sensing and actuator limitations as well as simulation and validation.[1] Recent interests have been motivated by the understanding that inspection and servicing vehicles must engage with unprepared clients. This realization opens a relatively new and untouched regime of research, and understanding how the absence of client cooperation influences the overall mission design, and how such a mission design is augmented when it is understood that the client can produce uncertain maneuvering, is an important question that must be answered. These scenario are challenging, and the enabling technologies are underdeveloped, when compared to the autonomous capabilities of spacecraft executing on-orbit inspection and servicing with fully operational and prepared clients, capable of assisting an approaching space vehicle.

Operational clients prepared for orbital rendezvous are typically capable of communicating helpful telemetry data and would nominally be equipped with distinguishing fiducials for an approaching spacecraft to perceive with an appropriate sensor suite, e.g., antennas, retroreflectors, reflective tape, LEDs, and visual and infrared features; on the contrary, a spacecraft approaching unprepared, potentially malfunctioning clients would be limited to silhouettes, edges, corners and points as visual aids and of course, would not be able to transmit helpful telemetry data.[2] This challenge is exacerbated if there is no *a priori* state information of a prospective client, due to either significant uncertainty in ground station observations or unplanned or uncontrolled maneuvers imparted on the client, moving it off its nominal trajectory. In such a case, the orbital state of the client vehicle may only be known to an accuracy of several kilometers.[3]

SATELLITE DYNAMIC MODELING AND PROBLEM FORMULATION

This analysis assumes that the inspection vehicle has been positioned in proximity of a designated client, whose absolute orbital state is either partially or entirely unknown due to its malfunctioning nature. The nature of the client also suggests the potential for uncertain maneuvering, both translational maneuvering or uncontrolled tumbling. In this section, the line-of-sight (LOS)-based coordinate system will first be introduced and the significance of this approach and its relevance to the satellite relative position control problem with malfunctioning clients will also be discussed. Then the LOS-based relative motion dynamics will be derived, formulated in a general second order form with considerations for uncertain client maneuvering.

Coordinate Frames and Client's Attitude Dynamics

It is more appropriate to build the dynamic equations of relative motion in a frame attached to the inspection vehicle as opposed to the client, due to the uncertain and malfunctioning nature of the client whose absolute orbital state is likely unknown. Moreover, this approach utilizes the relative navigation information directly within the dynamic equations of relative motion, avoiding the computational overhead of converting the navigation information to an equivalent Cartesian frame.[4,5] To appropriately define the LOS-based coordinate system, several intermediate frames must be established first; these coordinate frames are also depicted in Figure 1.

1. The Earth Centered Inertial (ECI) reference frame is defined as a coordinate frame attached to the Earth's center of mass, written as $\mathcal{I} = (x_\mathcal{I}, y_\mathcal{I}, z_\mathcal{I})$ and defined with respect to the Earth Mean Equinox (EME2000). The $x_\mathcal{I} - y_\mathcal{I}$ plane defines the equatorial plane, with $x_\mathcal{I}$ pointing through the vernal equinox and $z_\mathcal{I}$ pointing through the North Pole.[6,7]

2. The client's body-fixed frame is defined as the coordinate frame fixed to the client's center of mass, written as $\mathcal{B} = (x_\mathcal{B}, y_\mathcal{B}, z_\mathcal{B})$. The client's attitude quaternion is defined as $(\boldsymbol{q}_c, q_{c0}) \in \mathbb{R}^3 \times \mathbb{R}$, which defines the relationship between the client's body-fixed frame and the defined Earth Centered Inertial frame.

With these frames in mind, the relative state of the client can now be written using the navigation information directly, i.e, using the range (ρ), and two LOS angles, azimuth and elevation (θ, ε), to form the LOS-based state vector $\mathbf{x} = (\rho,\ \theta,\ \varepsilon)$, defined in the LOS-based coordinate system. Written as $\mathcal{L} = (x_\mathcal{L}, y_\mathcal{L}, z_\mathcal{L})$, and defined along the LOS range vector, the LOS-based coordinate frame is related to the client's body frame

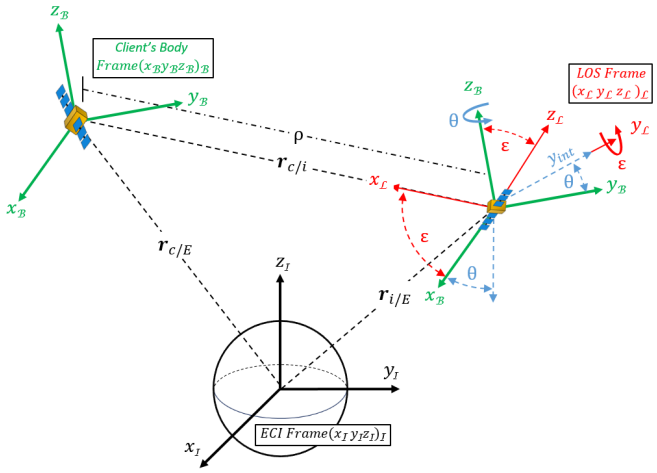

Figure 1: Line-Of-Sight Coordinate Frame

through two rotations, an initial rotation about $z_{\mathcal{B}}$ by θ, followed by a second rotation about y_{int} of the intermediate frame by -ε, where $\theta \in (-\pi, \pi)$ and $\varepsilon \in (-\pi/2, \pi/2)$, with the final degree of rotation being fixed, as described in Eq. (7).

The LOS-based coordinate frame transformation from the inertial ECI frame is defined by two transformations. That being an initial transformation from the $\mathcal{I}$ (inertial ECI) frame to the client's $\mathcal{B}$ (body-fixed) frame, followed by a second transformation from the client's $\mathcal{B}$ (body-fixed) frame to the inspector's $\mathcal{L}$ (LOS-based) frame. This transformation is written as

$$\overset{\mathcal{I}}{\mathcal{L}}\mathbf{R} = \overset{\mathcal{B}}{\mathcal{L}}\mathbf{R}\,\overset{\mathcal{I}}{\mathcal{B}}\mathbf{R}. \tag{1}$$

The transformation from the inertial ECI frame to the client's body-fixed frame ($\overset{\mathcal{I}}{\mathcal{B}}\mathbf{R}$), otherwise known as the direction cosine matrix (DCM), can be defined as a function of the client's attitude quaternion, and can be written as

$$\overset{\mathcal{I}}{\mathcal{B}}\mathbf{R} = (q_{c0}^2 - \mathbf{q}_c'\mathbf{q}_c)\mathbf{I}_{3\times 3} + 2\mathbf{q}_c'\mathbf{q}_c - q_{c0}\mathbf{q}_c^{\times}. \tag{2}$$

The client's attitude dynamics are described as (see Reference 8):

$$\boldsymbol{J}_c\,{}^{\mathcal{I}}\dot{\boldsymbol{\omega}}_c^{\mathcal{B}} = -{}^{\mathcal{I}}\boldsymbol{\omega}_c^{\mathcal{B}\times}\boldsymbol{J}_c\,{}^{\mathcal{I}}\boldsymbol{\omega}_c^{\mathcal{B}} + {}^{\mathcal{B}}\boldsymbol{\tau}_c + {}^{\mathcal{B}}\mathbf{T}_{d_c}, \tag{3}$$

$$\dot{\mathbf{q}}_c = \frac{1}{2}(\mathbf{q}_c^{\times} + q_{c0}\mathbf{I}_{3\times 3})\,{}^{\mathcal{I}}\boldsymbol{\omega}_c^{\mathcal{B}}, \tag{4}$$

$$\dot{q}_{c0} = \frac{1}{2}\mathbf{q}_c^T\,{}^{\mathcal{I}}\boldsymbol{\omega}_c^{\mathcal{B}}, \tag{5}$$

where ${}^{\mathcal{I}}\boldsymbol{\omega}_c^{\mathcal{B}} \in \mathbb{R}^3$ denotes the angular velocity of the client, expressed in the client's body-fixed frame, being read as the angular velocity of the body-fixed frame of the client about the inertial ECI frame. The client's inertia matrix is defined as $\boldsymbol{J}_c \in \mathbb{R}^{3\times 3}$. The quantities $\mathbf{q}_c^{\times}$ and ${}^{\mathcal{I}}\boldsymbol{\omega}_c^{\mathcal{B}\times}$ define skew-symmetric matrices, whose off diagonal elements are defined by their respective vectors. With that being said, recall the skew symmetric property is defined as

$$\boldsymbol{\omega}^{\times} = \begin{bmatrix} 0 & -\omega_3 & \omega_2 \\ \omega_3 & 0 & -\omega_1 \\ -\omega_2 & \omega_1 & 0 \end{bmatrix}, \tag{6}$$

whose off diagonal elements are defined by an arbitrary vector $\boldsymbol{\omega} = [\omega_1,\, \omega_2,\, \omega_3]^T$. The client's control torque and external disturbances expressed in the client's body-fixed frame are defined as ${}^{\mathcal{B}}\boldsymbol{\tau}_c = [{}^{\mathcal{B}}\tau_{c_1},\, {}^{\mathcal{B}}\tau_{c_2},\, {}^{\mathcal{B}}\tau_{c_3}]^T$ and ${}^{\mathcal{B}}\mathbf{T}_{d_c} = [{}^{\mathcal{B}}T_{d_{c1}},\, {}^{\mathcal{B}}T_{d_{c2}},\, {}^{\mathcal{B}}T_{d_{c3}}]^T$ respectively, where the left superscript notation indicates the relevant frame for force and torque terms. The client's control torque and external disturbances are bounded by the following assumption:

Assumption 1. *There exist unknown positive constants b_0 and b_1 which define the upper bounds of the client's control torque and external disturbance terms such that the inequalities $\|{}^{\mathcal{B}}\boldsymbol{\tau}_c\| \leq b_0$ and $\|{}^{\mathcal{B}}\mathbf{T}_{d_c}\| \leq b_1$ are satisfied.*

Finally, the transformation matrix which relates the LOS coordinate frame to the client's body-fixed coordinate frame (${}^{\mathcal{B}}_{\mathcal{L}}\mathbf{R}$), is written as

$$\begin{aligned} {}^{\mathcal{B}}_{\mathcal{L}}\mathbf{R} &= \begin{bmatrix} \cos(-\varepsilon) & 0 & \sin(-\varepsilon) \\ 0 & 1 & 0 \\ \sin(-\varepsilon) & 0 & \cos(-\varepsilon) \end{bmatrix} \begin{bmatrix} \cos(\theta) & \sin(\theta) & 0 \\ -\sin(\theta) & \cos(\theta) & 0 \\ 0 & 0 & 1 \end{bmatrix} \\ &= \begin{bmatrix} \cos(\varepsilon)\cos(\theta) & \cos(\varepsilon)\sin(\theta) & \sin(\varepsilon) \\ -\sin(\theta) & \cos(\theta) & 0 \\ -\sin(\varepsilon)\cos(\theta) & -\sin(\varepsilon)\sin(\theta) & cos(\varepsilon) \end{bmatrix}, \end{aligned} \tag{7}$$

where the following assumption is assumed satisfied:

Assumption 2. *To theoretically guarantee the existence of ${}^{\mathcal{B}}_{\mathcal{L}}\mathbf{R}$, the inequalities $\|{}^{\mathcal{B}}_{\mathcal{L}}\mathbf{R}\| \leq b_2$ and $\|{}^{\mathcal{B}}_{\mathcal{L}}\dot{\mathbf{R}}\| \leq b_3$ are assumed satisfied by some unknown positive constants b_2 and b_3, with ${}^{\mathcal{B}}_{\mathcal{L}}\mathbf{R}$ being defined by two rotations that satisfy $\theta \in (-\pi, \pi)$ and $\varepsilon \in (-\pi/2, \pi/2)$.*

Dynamic Equations of Relative Motion and Problem Formulation

In this section, the client's relative motion dynamics will be derived and discussed in the context of the LOS-based coordinate system defined in the previous section. To derive the LOS-based equations of relative motion, one must first apply the transport theorem, taking the second derivative of the position vector

$$\mathbf{r}_{c/E} = \mathbf{r}_{i/E} + \mathbf{r}_{c/i}, \tag{8}$$

with respect to the inertial frame. As shown in Figure 1, the quantity $\mathbf{r}_{i/E}$ denotes the inspector's position relative to the Earth. Similarly, the quantity $\mathbf{r}_{c/E}$ denotes the client's position relative to the Earth. Moreover, the quantity $\mathbf{r}_{c/i}$ denotes the position of the client with respect to the inspector, with the client's range defined as $||\mathbf{r}_{c/i}|| = \rho$. Similar to prior works (see References 4 and 5), standard vector notation is used, where the client, inspector and Earth are denoted by subscripts *c*, *i* and *E* respectively. Applying the transport theorm to Eq. (8), one has

$${}^{\mathcal{I}}\ddot{\mathbf{r}}_{c/E} = {}^{\mathcal{I}}\ddot{\mathbf{r}}_{i/E} + {}^{\mathcal{L}}\ddot{\mathbf{r}}_{c/i} + {}^{\mathcal{I}}\dot{\boldsymbol{\omega}}^{\mathcal{L}} \times \mathbf{r}_{c/i} + 2{}^{\mathcal{I}}\boldsymbol{\omega}^{\mathcal{L}} \times {}^{\mathcal{L}}\dot{\mathbf{r}}_{c/i} + {}^{\mathcal{I}}\boldsymbol{\omega}^{\mathcal{L}} \times ({}^{\mathcal{I}}\boldsymbol{\omega}^{\mathcal{L}} \times \mathbf{r}_{c/i}), \tag{9}$$

with bolded text indicating vector notation. For completeness, reference frames are introduced into the notation when discussing velocity or acceleration quantities–e.g., velocity vector ${}^{\mathcal{L}}\dot{\mathbf{r}}_{c/i}$ is read as the velocity of the client relative to the inspector with respect to the LOS frame. The client's relative position, velocity and acceleration quantities, written in the inspector's LOS frame are described as

$$\mathbf{r}_{c/i} = \begin{bmatrix} \rho \\ 0 \\ 0 \end{bmatrix},\ {}^{\mathcal{L}}\dot{\mathbf{r}}_{c/i} \begin{bmatrix} \dot{\rho} \\ 0 \\ 0 \end{bmatrix},\ {}^{\mathcal{L}}\ddot{\mathbf{r}}_{c/i} = \begin{bmatrix} \ddot{\rho} \\ 0 \\ 0 \end{bmatrix} \tag{10}$$

respectivly. The angular velocity and acceleration vectors of the LOS frame with respect to the inertial ECI frame can be expressed within the LOS frame as

$$
{}^{\mathcal{I}}\boldsymbol{\omega}^{\mathcal{L}} = \begin{bmatrix} \dot{\theta}\sin(\varepsilon) \\ -\dot{\varepsilon} \\ \dot{\theta}\cos(\varepsilon) \end{bmatrix} + {}^{\mathcal{B}}_{\mathcal{L}}\mathbf{R}\,{}^{\mathcal{I}}\boldsymbol{\omega}^{\mathcal{B}}_{c} \in \mathbb{R}^3, \tag{11}
$$

$$
{}^{\mathcal{I}}\dot{\boldsymbol{\omega}}^{\mathcal{L}} = \begin{bmatrix} \ddot{\theta}\sin(\varepsilon) + \dot{\theta}\dot{\varepsilon}\cos(\varepsilon) \\ -\ddot{\varepsilon} \\ \ddot{\theta}\cos(\varepsilon) - \dot{\theta}\dot{\varepsilon}\sin(\varepsilon) \end{bmatrix} + {}^{\mathcal{B}}_{\mathcal{L}}\dot{\mathbf{R}}\,{}^{\mathcal{I}}\boldsymbol{\omega}^{\mathcal{B}}_{c} + {}^{\mathcal{B}}_{\mathcal{L}}\mathbf{R}\,{}^{\mathcal{I}}\dot{\boldsymbol{\omega}}^{\mathcal{B}}_{c} \in \mathbb{R}^3, \tag{12}
$$

with

$$
{}^{\mathcal{B}}_{\mathcal{L}}\dot{\mathbf{R}} = -\,{}^{\mathcal{I}}\boldsymbol{\omega}^{\mathcal{B}\times}\,{}^{\mathcal{B}}_{\mathcal{L}}\mathbf{R}. \tag{13}
$$

The motion of the client relative to inspector within the ECI frame can now be derived using the absolute orbital dynamics of each spacecraft. The absolute relative motion dynamics are written as

$$
\begin{aligned}
{}^{\mathcal{I}}\ddot{\mathbf{r}}_{c/i} &= {}^{\mathcal{I}}\ddot{\mathbf{r}}_{c/E} - {}^{\mathcal{I}}\ddot{\mathbf{r}}_{i/E} \\
&= -\left(\tfrac{\mu}{\|\mathbf{r}_{c/E}\|^3}\mathbf{r}_{c/E} - \tfrac{\mu}{\|\mathbf{r}_{i/E}\|^3}\mathbf{r}_{i/E}\right) + \frac{1}{m_i}\left(\tfrac{m_i}{m_c}{}^{\mathcal{I}}\boldsymbol{F}_c - ({}^{\mathcal{I}}\boldsymbol{F}_i + {}^{\mathcal{I}}\boldsymbol{F}_d)\right) \\
&= {}^{\mathcal{I}}\Delta\mathbf{g} + \frac{1}{m_i}\left(\tfrac{m_i}{m_c}{}^{\mathcal{I}}\boldsymbol{F}_c - ({}^{\mathcal{I}}\boldsymbol{F}_i + {}^{\mathcal{I}}\boldsymbol{F}_d)\right),
\end{aligned} \tag{14}
$$

where ${}^{\mathcal{I}}\boldsymbol{F}_c = [{}^{\mathcal{I}}\boldsymbol{F}_{c_1},\ {}^{\mathcal{I}}\boldsymbol{F}_{c_2},\ {}^{\mathcal{I}}\boldsymbol{F}_{c_3}]^T$ and ${}^{\mathcal{I}}\boldsymbol{F}_i = [{}^{\mathcal{I}}\boldsymbol{F}_{i_1},\ {}^{\mathcal{I}}\boldsymbol{F}_{i_2},\ {}^{\mathcal{I}}\boldsymbol{F}_{i_3}]^T$ define the unknown client maneuver and the inspector's control input respectively. The unknown external disturbance term which includes disturbances such as atmospheric drag, solar radiation pressure and plume impingement is written as ${}^{\mathcal{I}}\boldsymbol{F}_d = [{}^{\mathcal{I}}\boldsymbol{F}_{d_1},\ {}^{\mathcal{I}}\boldsymbol{F}_{d_2},\ {}^{\mathcal{I}}\boldsymbol{F}_{d_3}]^T$. The relative gravity differential term ${}^{\mathcal{I}}\Delta\mathbf{g} = [{}^{\mathcal{I}}\Delta\mathbf{g}_1,\ {}^{\mathcal{I}}\Delta\mathbf{g}_2,\ {}^{\mathcal{I}}\Delta\mathbf{g}_3]^T$ describes the gravity difference between the client and inspector within the inertial ECI frame, and is described as

$$
{}^{\mathcal{I}}\Delta\mathbf{g} = -\left(\tfrac{\mu}{\|\mathbf{r}_{c/E}\|^3}\mathbf{r}_{c/E} - \tfrac{\mu}{\|\mathbf{r}_{i/E}\|^3}\mathbf{r}_{i/E}\right), \tag{15}
$$

where μ defines Earth's standard gravitational parameter. The client and inspector's mass properties are defined as m_c and m_i respectively. Moreover, it's assumed that the position of the client, relative to the inspector is assumed small, i.e., $\|\mathbf{r}_{c/i}\| \ll \|\mathbf{r}_{i/E}\|$. Therefore, Eq. (15) can be written as

$$
\begin{aligned}
{}^{\mathcal{I}}\Delta\mathbf{g} &= -\frac{\mu}{\|\mathbf{r}_{i/E}\|^3}\left(\tfrac{\|\mathbf{r}_{i/E}\|^3}{\|\mathbf{r}_{i/E}+\mathbf{r}_{c/i}\|^3}(\mathbf{r}_{i/E}+\mathbf{r}_{c/i}) - \mathbf{r}_{i/E}\right) \\
&= -\frac{\mu}{\|\mathbf{r}_{i/E}\|^3}\left[\left(1 + \tfrac{2\mathbf{r}_{i/E}\mathbf{r}_{c/i}}{\|\mathbf{r}_{i/E}\|^2} + \tfrac{\|\,\mathbf{r}_{c/i}\|^2}{\|(\mathbf{r}_{i/E}\|^2}\right)^{-\frac{3}{2}}(\mathbf{r}_{i/E}+\mathbf{r}_{c/i}) - \mathbf{r}_{i/E}\right] \\
&\approx -\frac{\mu}{\|\mathbf{r}_{i/E}\|^3}\left[\left(1 + 2\tfrac{\mathbf{r}_{i/E}\cdot\mathbf{r}_{c/i}}{\|\mathbf{r}_{i/E}\|^2}\right)(\mathbf{r}_{i/E}+\mathbf{r}_{c/i}) - \mathbf{r}_{i/E}\right],
\end{aligned} \tag{16}
$$

which can then be approximated using the Maclaurin expansion $(1+x)^{-\frac{3}{2}} = 1 - \frac{3x}{2} + \frac{15x^2}{8} - ...$ as

$$
{}^{\mathcal{I}}\Delta\mathbf{g} \approx -\frac{\mu}{\|\mathbf{r}_{i/E}\|^3}\left(\mathbf{r}_{c/i} - 3\tfrac{\mathbf{r}_{i/E}\cdot\mathbf{r}_{c/i}}{\|\mathbf{r}_{i/E}\|^2}\mathbf{r}_{i/E}\right). \tag{17}
$$

It is reasonable to assume these uncertain terms are bounded, and to that end, the following Assumption is introduced.

Assumption 3. *It is assumed that the bounding information on the uncertain, and time-varying, client maneuver, external disturbance and gravity differential are all unknown, but known to exist, i.e., there exists some unknown positive constants, such that* ${}^{\mathcal{I}}\mathbf{F}_c \leq b_4$, ${}^{\mathcal{I}}\mathbf{F}_d \leq b_5$ *and* ${}^{\mathcal{I}}\Delta\mathbf{g} \leq b_6||\boldsymbol{x}||$.

Finally, by substituting Eq. (10) - Eq. (12), and the absolute orbit dynamics from Eq. (14) into Eq. (9), and applying the necessary frame transformations using Eq. (2) and Eq. (7), the LOS-based dynamic equations of relative motion can be stated in its general second-order form as

$$\mathbf{M}(\mathbf{x})\ddot{\mathbf{x}} + \mathbf{F}(\mathbf{x}, \dot{\mathbf{x}}) = \boldsymbol{\psi}_d - \mathbf{u}(t), \tag{18}$$

with the inertia matrix defined as $\mathbf{M}(\mathbf{x}) = (\mathbf{M}_0(\mathbf{x}) + \Delta\mathbf{M}(\mathbf{x})) \in \mathbb{R}^{3\times3}$ and the lumped Coriolis and centripetal forcing terms defined as $\mathbf{F}(\mathbf{x}, \dot{\mathbf{x}}) = (\mathbf{F}_0(\mathbf{x}, \dot{\mathbf{x}}) + \Delta\mathbf{F}(\mathbf{x}, \dot{\mathbf{x}})) \in \mathbb{R}^3$; the terms $\mathbf{M}_0(\mathbf{x})$ and $\mathbf{F}_0(\mathbf{x}, \dot{\mathbf{x}})$ define the nominal terms, and $\Delta\mathbf{M}(\mathbf{x})$ and $\Delta\mathbf{F}(\mathbf{x}, \dot{\mathbf{x}})$ define uncertain terms. The following assumptions are made regarding the relative motion dynamic model

Assumption 4. *The model parameters* $\mathbf{M}(\mathbf{x})$ *and* $\mathbf{F}(\mathbf{x}, \dot{\mathbf{x}})$ *are bounded such that the following inequalities hold:*

$$\begin{aligned} &\mathbf{M}(\mathbf{x}) \leq b_7 \\ &\mathbf{F}(\mathbf{x}, \dot{\mathbf{x}}) \leq b_8 + b_9||\mathbf{x}|| + b_{10}||\dot{\mathbf{x}}||^2. \end{aligned} \tag{19}$$

The quantity $\boldsymbol{\psi}_d$, is a lumped uncertain term, containing the gravitational differential (${}^{\mathcal{L}}\Delta\mathbf{g}$), client thrusting (${}^{\mathcal{L}}\boldsymbol{F}_c$), external disturbance quantities (${}^{\mathcal{L}}\boldsymbol{F}_d$ and ${}^{\mathcal{B}}\mathbf{T}_{d_c}$) and client control torque (${}^{\mathcal{B}}\boldsymbol{\tau}_c$). The quantities $\mathbf{M}(\mathbf{x})$, $\mathbf{F}(\mathbf{x}, \dot{\mathbf{x}})$ and $\boldsymbol{\psi}_d$ are defined as

$$\mathbf{M}(\mathbf{x}) = m_i \begin{bmatrix} 1 & 0 & 0 \\ 0 & \rho\cos\varepsilon & 0 \\ 0 & 0 & \rho \end{bmatrix}, \tag{20}$$

$$\begin{aligned} \mathbf{F}(\mathbf{x}, \dot{\mathbf{x}}) = m_i \begin{bmatrix} 0 \\ -\rho\dot{\theta}\dot{\varepsilon}sin\varepsilon \\ 0 \end{bmatrix} + m_i \left({}^{\mathcal{B}}_{\mathcal{L}}\dot{\mathbf{R}}\, {}^{\mathcal{I}}\boldsymbol{\omega}^{\mathcal{B}}_c - {}^{\mathcal{B}}_{\mathcal{L}}\mathbf{R}\, \boldsymbol{J}_c^{-1}\, {}^{\mathcal{I}}\boldsymbol{\omega}^{\mathcal{B}\times}_c \boldsymbol{J}_c\, {}^{\mathcal{I}}\boldsymbol{\omega}^{\mathcal{B}}_c \right) \times \mathbf{r}_{c/i} \\ + 2m_i {}^{\mathcal{I}}\boldsymbol{\omega}^{\mathcal{L}} \times {}^{\mathcal{L}}\dot{\mathbf{r}}_{c/i} + m_i {}^{\mathcal{I}}\boldsymbol{\omega}^{\mathcal{L}} \times ({}^{\mathcal{I}}\boldsymbol{\omega}^{\mathcal{L}} \times \mathbf{r}_{c/i}), \end{aligned} \tag{21}$$

and

$$\begin{aligned} \boldsymbol{\psi}_d = m_i {}^{\mathcal{L}}\Delta\mathbf{g} + \frac{m_i}{m_c} {}^{\mathcal{L}}\boldsymbol{F}_c - {}^{\mathcal{L}}\boldsymbol{F}_d - m_i\, {}^{\mathcal{B}}_{\mathcal{L}}\mathbf{R}\, \boldsymbol{J}_c^{-1}({}^{\mathcal{B}}\mathbf{T}_{d_c} \times r_{c/i}) \\ - m_i\, {}^{\mathcal{B}}_{\mathcal{L}}\mathbf{R}\, \boldsymbol{J}_c^{-1}({}^{\mathcal{B}}\boldsymbol{\tau}_c \times r_{c/i}) \end{aligned} \tag{22}$$

respectively. Recall that the client's relative position can be expressed using the spherical based LOS coordinates, by denoting the relative position vector $\mathbf{x} = [\rho,\ \theta,\ \varepsilon]^T$. Moreover, the inspector's thrust vector in the LOS-based frame, previously written as ${}^{\mathcal{L}}\boldsymbol{F}_i$, is denoted as $\mathbf{u}(t) = [u_1,\ u_2,\ u_3]^T$. Now, the second order dynamic expression from Eq. (18) can be written as

$$\mathbf{M}_0(\mathbf{x})\ddot{\mathbf{x}} + \mathbf{F}_0(\mathbf{x}, \dot{\mathbf{x}}) = \boldsymbol{\psi}_D - \mathbf{u}(t), \tag{23}$$

with the new lumped uncertain term $\boldsymbol{\psi}_D$ written as

$$\boldsymbol{\psi}_D = -\Delta\mathbf{M}(\mathbf{x})\ddot{\mathbf{x}} - \Delta\mathbf{F}(\mathbf{x}, \dot{\mathbf{x}}) + \boldsymbol{\psi}_d, \tag{24}$$

which now contains the system uncertain terms $\Delta\mathbf{M}(\mathbf{x})$ and $\Delta\mathbf{F}(\mathbf{x}, \dot{\mathbf{x}})$. Based on Assumptions 1 - 4 the following assumption holds:

Assumption 5. *The lumped uncertain term $\boldsymbol{\psi}_D$ can be bounded by the following inequality:*

$$||\boldsymbol{\psi}_D|| \leq a_0 + a_1||\boldsymbol{x}|| + a_2||\dot{\boldsymbol{x}}||^2, \tag{25}$$

where a_j $(j = 0,\ 1,\ 2)$ are unknown positive constants.

CONTROL SCHEME

In this section, a robust adaptive second-order fast non-singular terminal sliding mode control (ASOFNTSMC) scheme is proposed to compensate for system uncertainties and disturbances without prior bounding knowledge. The proposed control scheme avoids the singularity problem inherent to terminal sliding mode control (TSMC) and ensures the control profile is tractable; fast, finite-time convergence is also guaranteed, ensuing the error states converge to zero while simultaneously reducing detrimental chattering effects.

Preliminaries

Throughout this paper, when discussing the designed sliding manifolds the following notation is proposed for simplicity:

$$\mathrm{sig}^{\lambda}(\mathbf{v}) = (|v_1|^{\lambda}\mathrm{sign}(v_1), \ldots,\ |v_n|^{\lambda}\mathrm{sign}(v_n))^T, \tag{26}$$

where $\mathbf{v} = [v_1, v_2, ..., v_n]^T \in \mathbb{R}^n$ and $|\mathbf{v}|^{\lambda} = [|\mathbf{v}_1|^{\lambda}, |\mathbf{v}_2|^{\lambda}, ..., |\mathbf{v}_n|^{\lambda}]^T \in \mathbb{R}^n$ for some positive constant λ. An important lemma can also introduced.

Lemma 1. *The zero solution of the nonlinear dynamics is finite-time stable if it is both stable in the sense of Lyapunov, and finite-time convergent.[9] With this understanding, a Lyapunov description of finite-time stability is proposed. Suppose there exists a function $V(x)$ that is positive-definite on $\hat{U}$ and defined in the neighborhood $\hat{U} \subset \mathbb{R}^n$ such that*

$$\dot{V}(\boldsymbol{x}) = -\alpha V(\boldsymbol{x}) - \beta V^{\phi}(\boldsymbol{x}), \quad 0 < \phi < 1 \tag{27}$$

is negative semi-definite on $\hat{U}$ for some positive constants α and β. Then the nonlinear system is said to be finite-time stable with a settling time given by

$$T_s \leq \frac{1}{\alpha(1-\phi)} \ln \frac{\alpha V^{1-\phi}(\boldsymbol{x}(0)) + \beta}{\beta}, \tag{28}$$

for any given initial condition $V(\boldsymbol{x}(0))$. However, if $\hat{U} \subset \mathbb{R}^n$ and $V(\boldsymbol{x})$ are radially unbounded then the origin is said to be globally finite-time stable.[10]

Sliding Manifold Design

Conventional sliding mode control (SMC) benefits from a relatively simple implementation compared to other nonlinear control techniques, and benefits from strong robustness properties with respect to model uncertainties and external disturbances. SMC is two phase process to drive the trajectories of the sliding variables to a predefined manifold, known as the sliding manifold where the behavior on this manifold is entirely independent of matched uncertainties. The two phases of SMC involve a reaching phase and a sliding phase. During the reaching phase the control law drives the trajectories of the sliding variables to the sliding manifold, after arriving, the sliding phase begins, constraining the trajectories of the system to the designed manifold where the original dynamics are well behaved. Once the sliding variables converge to the defined manifold the error states will converge to zero exponentially, this process is depicted in Figure 2.

However, SMC inherently suffers from chattering effects, due to the discontinuous nature of conventional SMC. In practical applications, SMC will only drive the trajectories of the system to the real sliding mode,

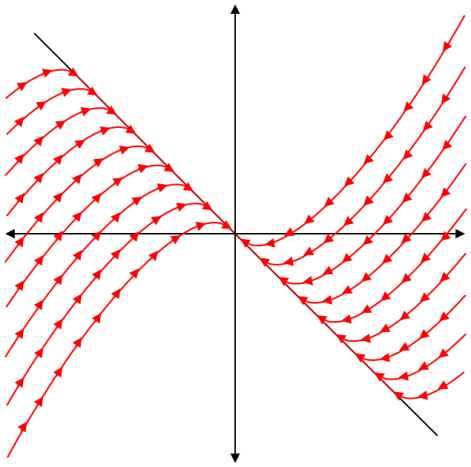

Figure 2: Phase Portrait: Sliding Manifold s = 0 (black) and System Trajectories (red)

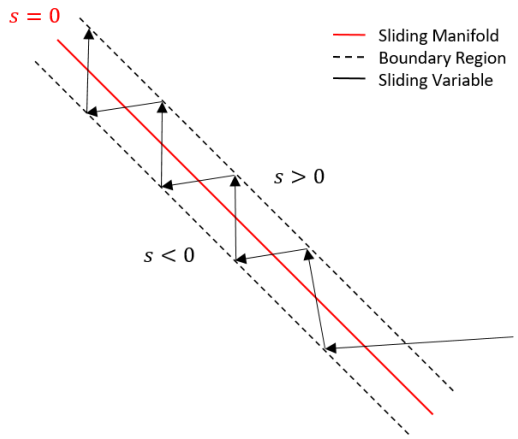

Figure 3: Behavior of the Sliding Variables Near the Designed Manifold

which is a region around the sliding manifold and because of this, rapid switching above and below the sliding manifold occurs. This phenomenon is caused by time delays between when the control signal is produced, and when the control signal is felt by the system. This causes high heat loss in electronic power circuits and degrades system hardware, which in turn causes reduced control accuracy and degrades system performance.[11] The chattering behaves as shown in Figure 3, depicting the trajectories of the sliding variables bouncing above and below the sliding manifold. This phenomenon can be mitigated or practically eliminated through various techniques, a popular method is to approximate the discontinuous signum function via a high slope saturation function or hyperbolic tangent function. Other techniques include designing mitigating characteristics into the sliding manifold itself or developing adaptive procedures to dynamically tune the system's control input.

With that in mind, the proposed manifold design is comprised of a proportional-derivative sliding mode (PDSM) manifold and a fast nonsingular terminal sliding mode (FNTSM) manifold to achieve faster convergence of the tracking errors and help mitigate adverse chattering effects; together, these manifolds form a SOFNTSM manifold. The proposed PDSM manifold $\mathbf{s}_1$ and FNTSM manifold $\mathbf{s}_2$ are defined as

$$\mathbf{s}_1 = \dot{\mathbf{e}} + \mathbf{K}_1\mathbf{e} \tag{29}$$

and

$$\mathbf{s}_2 = \mathbf{s}_1 + \mathbf{K}_2\text{sig}^{\gamma_2}(\mathbf{s}_1) + \mathbf{K}_3\text{sig}^{\gamma_1}(\dot{\mathbf{s}}_1) \tag{30}$$

respectively, where the tracking error $\mathbf{e} \in \mathbb{R}^3$, is defined as $\mathbf{e} = \mathbf{x} - \mathbf{x}_d$ with the desired state vector $\mathbf{x}_d \in \mathbb{R}^3$ defined as $\mathbf{x}_d = \begin{bmatrix}\rho_d,\ \theta_d,\ \varepsilon_d\end{bmatrix}^T$. The parameters $\mathbf{K}_1$, $\mathbf{K}_2$ and $\mathbf{K}_3$ are positive-definite design matrices written as $\mathbf{K}_1 = \text{diag}(k_{11},\ k_{12},\ k_{13})$ for $k_{1j} > 0\ (j = 1,\ 2,\ 3)$, $\mathbf{K}_2 = \text{diag}(k_{21},\ k_{22},\ k_{23})$ for $k_{2j} > 0\ (j = 1,\ 2,\ 3)$ and $\mathbf{K}_3 = \text{diag}(k_{31},\ k_{32},\ k_{33})$ for $k_{3j} > 0\ (j = 1,\ 2,\ 3)$ respectively. The design constants γ_1 and γ_2 are positive constants satisfying $1 < \gamma_1 < 2$ such that the inequality $\gamma_2 > \gamma_1$ is satisfied. The design parameters expressed in Eq. (29) and Eq. (30) can be used to adjust the reaching time to the SOFNTSM manifold $\mathbf{s}_2 = 0$, such that

$$\mathbf{s}_1 + \mathbf{K}_2\text{sig}^{\gamma_2}(\mathbf{s}_1) + \mathbf{K}_3\text{sig}^{\gamma_1}(\dot{\mathbf{s}}_1) = 0. \tag{31}$$

When the trajectories of sliding variable $\mathbf{s}_1$ are far from the designed PDSM manifold, the higher order terms of Eq. (31) will dominate and dictate the convergence rate of $\mathbf{s}_1$. Conversely, when the trajectories of sliding variable $\mathbf{s}_1$ are close to the designed PDSM manifold the first-order terms of Eq. (31) will primarily influence the convergence rate of $\mathbf{s}_1$.[12] The first derivative of FNTSM manifold can be expressed as

$$\begin{aligned}\dot{\mathbf{s}}_2 &= \dot{\mathbf{s}}_1 + \gamma_2\mathbf{K}_2\mathrm{diag}(|\mathbf{s}_1|^{\gamma_2-1})\dot{\mathbf{s}}_1 + \gamma_1\mathbf{K}_3\mathrm{diag}(|\dot{\mathbf{s}}_1|^{\gamma_1-1})\ddot{\mathbf{s}}_1 \\ &= \dot{\mathbf{s}}_1 + \gamma_2\mathbf{K}_2\mathrm{diag}(|\mathbf{s}_1|^{\gamma_2-1})\dot{\mathbf{s}}_1 + \gamma_1\mathbf{K}_3\mathrm{diag}(|\dot{\mathbf{s}}_1|^{\gamma_1-1})(-\dot{\mathbf{M}}_0^{-1}(\mathbf{x})\mathbf{F}_0(\mathbf{x},\dot{\mathbf{x}}) \\ &\quad - \mathbf{M}_0^{-1}(\mathbf{x})\dot{\mathbf{F}}_0(\mathbf{x},\dot{\mathbf{x}}) - \dot{\mathbf{M}}_0^{-1}(\mathbf{x})\mathbf{u}(t) - \mathbf{M}_0^{-1}(\mathbf{x})\dot{\mathbf{u}}(t) - \dddot{\mathbf{q}}_d \\ &\quad - \mathbf{K}_1\mathbf{M}_0^{-1}(\mathbf{x})\mathbf{F}_0(\mathbf{x},\dot{\mathbf{x}}) - \mathbf{K}_1\mathbf{M}_0^{-1}(\mathbf{x})\mathbf{u}(t) - \mathbf{K}_1\ddot{\mathbf{q}}_d + \overline{\boldsymbol{\psi}}_D),\end{aligned} \tag{32}$$

where

$$\overline{\boldsymbol{\psi}}_D = (\dot{\mathbf{M}}_0^{-1}(\mathbf{x}) + \mathbf{K}_1\mathbf{M}_0^{-1}(\mathbf{x}))\boldsymbol{\psi}_D + \mathbf{M}_0^{-1}(\mathbf{x})\dot{\boldsymbol{\psi}}_D. \tag{33}$$

Based on Assumptions 1 - 5 the following assumption holds:

Assumption 6. *The lumped uncertain term $\boldsymbol{\psi}_D$ can be bounded by the following inequality:*

$$||\overline{\boldsymbol{\psi}}_D|| \leq \kappa_0 + \kappa_1||\boldsymbol{x}|| + \kappa_2||\dot{\boldsymbol{x}}||^2, \tag{34}$$

where κ_j $(j = 0,\ 1,\ 2)$ are unknown positive constants.

Adaptive Second-Order Fast Nonsingular Terminal Sliding Mode Control

Using the defined manifolds, both the PDSM and FNTSM manifolds from Eq. (29) and Eq. (30) respectively, as well as the derived second order LOS-based dynamic model from Eq. (18), the proposed ASOFNTSMC scheme can be introduced as

$$\begin{aligned}\dot{\mathbf{u}}(t) =& \mathbf{M}_0(\mathbf{x})(-\dot{\mathbf{M}}_0^{-1}(\mathbf{x})\mathbf{F}_0(\mathbf{x},\dot{\mathbf{x}}) - \mathbf{M}_0^{-1}(\mathbf{x})\dot{\mathbf{F}}_0(\mathbf{x},\dot{\mathbf{x}}) - \dot{\mathbf{M}}_0^{-1}(\mathbf{x})\mathbf{u}(t) - \dddot{\mathbf{q}}_d - \mathbf{K}_1\mathbf{M}_0^{-1}(\mathbf{x})\mathbf{F}_0(\mathbf{x},\dot{\mathbf{x}}) \\ &- \mathbf{K}_1\mathbf{M}_0^{-1}(\mathbf{x})\mathbf{u}(t) - \mathbf{K}_1\ddot{\mathbf{q}}_d + \frac{\gamma_2}{\gamma_1}\mathbf{K}_3^{-1}\mathbf{K}_2\mathrm{diag}(|\mathbf{s}_1|^{\gamma_2-1})\mathrm{diag}(|\dot{\mathbf{s}}_1|^{2-\gamma_1})\mathrm{sign}(\dot{\mathbf{s}}_1) \\ &+ \frac{1}{\gamma_1}\mathbf{K}_3^{-1}\mathrm{diag}(|\dot{\mathbf{s}}_1|^{2-\gamma_1})\mathrm{sign}(\dot{\mathbf{s}}_1) + \mathbf{K}_4\mathbf{s}_2 + (\hat{\kappa}_0 + \hat{\kappa}_1||\mathbf{x}|| + \hat{\kappa}_2||\dot{\mathbf{x}}||^2)\mathrm{sign}(\mathbf{s}_2)),\end{aligned} \tag{35}$$

where $\hat{\kappa}_j$ $(j = 0,\ 1,\ 2)$ denotes the estimations of the bounding parameters in Eq. (34). A constant plus proportional rate reaching strategy is proposed, defined by $\mathbf{K}_4$ where $\mathbf{K}_4 = \mathrm{diag}(k_{41},\ k_{42},\ k_{43})$, with $k_{4j} > 0$ $(j = 1,\ 2,\ 3)$. This strategy forces the trajectories of the system onto the sliding manifold quicker when the sliding variables are far from the defined manifold.[13] The plus proportional rate reaching law encourages the trajectories of the sliding variables to approach the designed manifold for larger values $\mathbf{K}_4$. It is important to mention that Eq. (35) contains both the equivalent $(\dot{\mathbf{u}}_{eq}(t))$ and switching $(\dot{\mathbf{u}}_{sw}(t))$ control terms written as

$$\dot{\mathbf{u}}(t) = \dot{\mathbf{u}}_{eq}(t) + \dot{\mathbf{u}}_{sw}(t); \tag{36}$$

the ASOFNTSMC scheme can now be formalized as

$$\mathbf{u}(t) = \mathbf{u}_{eq}(t) + \mathbf{u}_{sw}(t) = \int_0^t (\dot{\mathbf{u}}_{eq}(t) + \dot{\mathbf{u}}_{sw}(t))\,dt. \tag{37}$$

The proposed ASOFNTSMC scheme is depicted in Figure 4. Contrary to conventional SMC, the discontinuous switching function is masked behind the control input's time derivative, which allows the control input to be continuous, while having chattering effectively eliminated without reducing the tracking precision.[14]

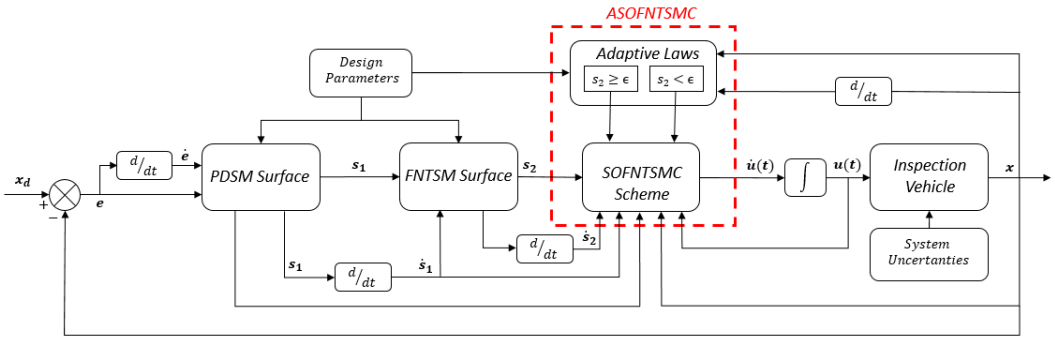

Figure 4: Control Diagram of the Proposed ASOFNTMC Scheme

In practice, the bounding information on system uncertainties and perturbations are hard to determine in advance. Therefore, an adaptive approach is necessary to enable the control to be properly attenuated throughout the simulation and to ensure the control scheme isn't overcompensating for the system uncertainties and perturbations as gain overestimation adversely effects system performance, degrading tracking error and amplifying system chattering. Moreover, without *a priori* knowledge of system uncertainties and perturbations the region of convergence is hard to determine beforehand.[15]

Recall that in practice SMC drives the trajectories of the sliding variables to a region around the sliding mode, called the real sliding mode. With this behavior in mind, as the designed control forces the trajectories of the sliding variables to the real sliding mode, it is possible for a potentially boundless increases in the adaptive parameters.[16] Therefore, the adaptive framework is proposed in the context of the real sliding mode, defined by ϵ, which defines the region around the sliding mode ($\mathbf{s}_2 = 0$). With this in mind, and based on Assumption 6, the adaptive framework is proposed as

$$\dot{\hat{\kappa}}_0 = \begin{Bmatrix} \gamma_1 \bar{\kappa}_0 \|\mathbf{s}_2^T \mathbf{K}_3 \mathrm{diag}(|\dot{\mathbf{s}}_1|^{\gamma_1 - 1})\|, & \|\mathbf{s}_2\| \geq \epsilon \\ 0, & \|\mathbf{s}_2\| < \epsilon \end{Bmatrix} \tag{38}$$

$$\dot{\hat{\kappa}}_1 = \begin{Bmatrix} \gamma_1 \bar{\kappa}_1 \|\mathbf{s}_2^T \mathbf{K}_3 \mathrm{diag}(|\dot{\mathbf{s}}_1|^{\gamma_1 - 1})\| \|\mathbf{x}\|, & \|\mathbf{s}_2\| \geq \epsilon \\ 0, & \|\mathbf{s}_2\| < \epsilon \end{Bmatrix} \tag{39}$$

$$\dot{\hat{\kappa}}_2 = \begin{Bmatrix} \gamma_1 \bar{\kappa}_2 \|\mathbf{s}_2^T \mathbf{K}_3 \mathrm{diag}(|\dot{\mathbf{s}}_1|^{\gamma_1 - 1})\| \|\dot{\mathbf{x}}\|^2, & \|\mathbf{s}_2\| \geq \epsilon \\ 0, & \|\mathbf{s}_2\| < \epsilon \end{Bmatrix}, \tag{40}$$

with the positive constants $\bar{\kappa}_0$, $\bar{\kappa}_1$, $\bar{\kappa}_2$ defining the adaptive rates. The proposed ASOFNTSMC law can be supplemented with a high slope saturation function, in the form of a hyperbolic tangent function to improve control performance and eliminate residual chattering effects during the real sliding mode. Therefore, to eliminate residual chattering in Eq. (35), the discontinuous switching function $\mathrm{sign}(\mathbf{s}_2)$ can be replaced with the continuous $\tanh(\frac{\mathbf{s}_2}{\delta})$ function, where $\delta > 0$ is a sufficiently small constant that defines the inflection point of the hyperbolic tangent function; a larger value of $\delta > 0$ attenuates chattering effects, but at the expense of steady state error.[5, 17]

The validity of the proposed ASOFNTSMC algorithm can now be presented in the context of Lyapunov stability

Theorem 2. *Considering the LOS-based dynamic model (Eq.* (23)*), the PDSM and FNTSM manifolds (Eq.* (29) *and Eq.* (30)*), proposed ASOFNTSMC scheme (Eq.* (35)*) and the adaptation process defined in Eq.* (38) *- Eq.* (40)*, it can be proven that the sliding modes are established in finite-time and that the error states are bounded and converge to a region around their desired states exponentially.*

Proof. Consider the following positive definite Lyapunov candidate function, written as

$$V = \frac{1}{2}\mathbf{s}_2^T\mathbf{s}_2 + \frac{1}{2}\sum_{j=0}^{2}\bar{\kappa}_j^{-1}\tilde{\kappa}_j^2, \tag{41}$$

with $\tilde{\kappa}_j = \hat{\kappa}_j - \kappa_j$ $(j = 0,\ 1,\ 2)$ defining the adaptive errors. Recall from Eq. (34), κ_j $(j = 0,\ 1,\ 2)$ denote the unknown positive constants defining the upper bound of the system uncertainties, with $\hat{\kappa}_j$ $(j = 0,\ 1,\ 2)$ denoting their estimations using Eq. (38) - Eq. (40). Taking the time derivative of Eq. (41), one has

$$\dot{V} = \mathbf{s}_2^T\dot{\mathbf{s}}_2 + \sum_{j=0}^{2}\bar{\kappa}_j^{-1}\tilde{\kappa}_j\dot{\hat{\kappa}}_j. \tag{42}$$

Making the necessary substitutions using Eq. (32) and Eq. (35) one has

$$\begin{aligned}
\dot{V} = {} & \mathbf{s}_2^T(\dot{\mathbf{s}}_1 + \gamma_2\mathbf{K}_2\mathrm{diag}(|\mathbf{s}_1|^{\gamma_2-1})\dot{\mathbf{s}}_1 + \gamma_1\mathbf{K}_3\mathrm{diag}(|\dot{\mathbf{s}}_1|^{\gamma_1-1})(-\dot{\mathbf{M}}_0^{-1}(\mathbf{x})\mathbf{F}_0(\mathbf{x},\dot{\mathbf{x}}) \\
& -\mathbf{M}_0^{-1}(\mathbf{x})\dot{\mathbf{F}}_0(\mathbf{x},\dot{\mathbf{x}}) - \dot{\mathbf{M}}_0^{-1}(\mathbf{x})\mathbf{u}(t) - \mathbf{M}_0^{-1}(\mathbf{x})\dot{\mathbf{u}}(t) - \ddot{\mathbf{q}}_d \\
& -\mathbf{K}_1\mathbf{M}_0^{-1}(\mathbf{x})\mathbf{F}_0(\mathbf{x},\dot{\mathbf{x}}) - \mathbf{K}_1\mathbf{M}_0^{-1}(\mathbf{x})\mathbf{u}(t) - \mathbf{K}_1\ddot{\mathbf{q}}_d + \overline{\boldsymbol{\psi}}_D)) + \sum_{j=0}^{2}\bar{\kappa}_j^{-1}\tilde{\kappa}_j\dot{\hat{\kappa}}_j \\
\dot{V} = {} & \gamma_1\mathbf{s}_2^T\mathbf{K}_3\mathrm{diag}(|\dot{\mathbf{s}}_1|^{\gamma_1-1})\overline{\boldsymbol{\psi}}_D - \gamma_1\mathbf{s}_2^T\mathbf{K}_3\mathbf{K}_4\mathrm{diag}(|\dot{\mathbf{s}}_1|^{\gamma_1-1})\mathbf{s}_2 \\
& -\gamma_1(\hat{\kappa}_0 + \hat{\kappa}_1||\mathbf{x}|| + \hat{\kappa}_2||\dot{\mathbf{x}}||^2)\mathbf{s}_2^T\mathbf{K}_3\mathrm{diag}(|\dot{\mathbf{s}}_1|^{\gamma_1-1})\mathrm{sign}(\mathbf{s}_2) + \sum_{j=0}^{2}\bar{\kappa}_j^{-1}\tilde{\kappa}_j\dot{\hat{\kappa}}_j.
\end{aligned} \tag{43}$$

Recalling the adaptive process is governed by Eq. (38) - Eq. (40) and the bounding inequality from Assumption 6, one then has

$$\begin{aligned}
\dot{V} \leq {} & \gamma_1\|\overline{\boldsymbol{\psi}}_D\|\|\mathbf{s}_2^T\mathbf{K}_3\mathrm{diag}(|\dot{\mathbf{s}}_1|^{\gamma_1-1})\| - \gamma_1\mathbf{s}_2^T\mathbf{K}_3\mathbf{K}_4\mathrm{diag}(|\dot{\mathbf{s}}_1|^{\gamma_1-1})\mathbf{s}_2 \\
& - \gamma_1(\hat{\kappa}_0 + \hat{\kappa}_1||\mathbf{x}|| + \hat{\kappa}_2||\dot{\mathbf{x}}||^2)\mathbf{s}_2^T\mathbf{K}_3\mathrm{diag}(|\dot{\mathbf{s}}_1|^{\gamma_1-1})\mathrm{sign}(\mathbf{s}_2) \\
& + \gamma_1\tilde{\kappa}_0\|\mathbf{s}_2^T\mathbf{K}_3\mathrm{diag}(|\dot{\mathbf{s}}_1|^{\gamma_1-1})\| + \gamma_1\tilde{\kappa}_1\|\mathbf{s}_2^T\mathbf{K}_3\mathrm{diag}(|\dot{\mathbf{s}}_1|^{\gamma_1-1})\|\|\mathbf{x}\| \\
& + \gamma_1\tilde{\kappa}_2\|\mathbf{s}_2^T\mathbf{K}_3\mathrm{diag}(|\dot{\mathbf{s}}_1|^{\gamma_1-1})\|\|\dot{\mathbf{x}}\|^2
\end{aligned} \tag{44}$$

$$\begin{aligned}
\dot{V} \leq {} & \gamma_1(\kappa_0 + \kappa_1||\mathbf{x}|| + \kappa_2||\dot{\mathbf{x}}||^2)\|\mathbf{s}_2^T\mathbf{K}_3\mathrm{diag}(|\dot{\mathbf{s}}_1|^{\gamma_1-1})\| - \gamma_1\mathbf{s}_2^T\mathbf{K}_3\mathbf{K}_4\mathrm{diag}(|\dot{\mathbf{s}}_1|^{\gamma_1-1})\mathbf{s}_2 \\
& - \gamma_1(\hat{\kappa}_0 + \hat{\kappa}_1||\mathbf{x}|| + \hat{\kappa}_2||\dot{\mathbf{x}}||^2)\|\mathbf{s}_2^T\mathbf{K}_3\mathrm{diag}(|\dot{\mathbf{s}}_1|^{\gamma_1-1})\| \\
& + \gamma_1(\tilde{\kappa}_0 + \tilde{\kappa}_1\|\mathbf{x}\| + \tilde{\kappa}_2\|\dot{\mathbf{x}}\|^2)\|\mathbf{s}_2^T\mathbf{K}_3\mathrm{diag}(|\dot{\mathbf{s}}_1|^{\gamma_1-1})\|,
\end{aligned}$$

which can be approximated as

$$\dot{V} = -\frac{c_0}{2}\mathbf{s}_2^T\mathbf{s}_2 - \frac{c_1}{\sqrt{2}}\|\mathbf{s}_2\|, \tag{45}$$

with c_0 and c_1 written as

$$c_0 = 2\gamma_1\lambda_{min}(\mathbf{K}_3\mathbf{K}_4\mathrm{diag}(|\dot{\mathbf{s}}_1|^{\gamma_1-1})), \tag{46}$$

and

$$
\begin{aligned}
c_1 = \sqrt{2}\gamma_1((\kappa_0 - \hat{\kappa}_0 + \tilde{\kappa}_0) + (\kappa_1 - \hat{\kappa}_1 + \tilde{\kappa}_1)||\mathbf{x}|| \\
+ (\kappa_2 - \hat{\kappa}_2 + \tilde{\kappa}_2)||\dot{\mathbf{x}}||^2)\lambda_{min}(\mathbf{K}_3\mathbf{K}_4\mathrm{diag}(|\dot{\mathbf{s}}_1|^{\gamma_1 - 1}))
\end{aligned} \tag{47}
$$

respectively. Eq. (45) can now be written as

$$
\dot{V} = -c_0 V - c_1 V^{\frac{1}{2}}, \tag{48}
$$

and from Lemma 1, one can conclude that the system is finite-time stable, completing the proof. For similar detailed derivations see References 12 and 14.

□

NUMERICAL RESULTS

To evaluate the utility and performance of the proposed ASOFNTSMC scheme for on-orbit servicing and inspection applications, three numerical simulations are performed using MATLAB/Simulink. For each Scenario it's assumed the client is malfunctioning, and therefore, incapable of actively aiding in a coordinated rendezvous maneuver. In Scenario 1, it's assumed the client is incapable of producing controlled maneuvers, however, it's assumed to be freely tumbling. In Scenario 2, the client is both freely tumbling and capable of producing uncertain maneuvering. Finally Scenario 3 demonstrates a phased approach to a freely tumbling non-maneuvering client.

In the context of each numerical simulation the inspection vehicle is assumed to be small ($m_i \approx 50$ kg), modeled as a point mass. Ideal thrusting is assumed, saturated at ± 5 N, without any thruster misalignments. Additionally, the client's inertia properties are defined as

$$
\boldsymbol{J}_c = \begin{bmatrix} 20.31 & 0 & 0 \\ 0 & 39.06 & 0 \\ 0 & 0 & 31.25 \end{bmatrix} \mathrm{kg} \cdot \mathrm{m}^2, \tag{49}
$$

with the client spacecraft's initial angular rate and initial attitude quaternion for the first two scenarios being defined as

$$
\boldsymbol{\omega}_c(0) = \begin{bmatrix} 0.3 & -0.1 & -0.5 \end{bmatrix}^T \tag{50}
$$

and

$$
\mathbf{q}_c(0) = \begin{bmatrix} 0 & -0.253 & 0 \end{bmatrix}^T \quad \mathbf{q}_{c0}(0) = \sqrt{1 - \mathbf{q}_c'(0)\mathbf{q}_c(0)} \tag{51}
$$

respectively. The initial angular rate and initial attitude quaternion for the third and final scenario is located in the respective section.

Moreover, for each Scenario the inspector is assumed to be positioned within close proximity of the client. With that being said, the initial states written in the LOS-based coordinate frame are defined as

$$
\mathbf{x}(0) = \begin{bmatrix} 100 \ \mathrm{m} \\ -1.260 \ \mathrm{rad} \\ 0.163 \ \mathrm{rad} \end{bmatrix} \tag{52}
$$

and

$$\dot{\mathbf{x}}(0) = \begin{bmatrix} -1.640 \times 10^{-2} \ \dfrac{\mathrm{m}}{\mathrm{s}} \\ -0.484 \times 10^{-3} \ \dfrac{\mathrm{rad}}{\mathrm{s}} \\ 0.253 \times 10^{-3} \ \dfrac{\mathrm{rad}}{\mathrm{s}} \end{bmatrix}. \tag{53}$$

respectively.

The client and inspector's orbital elements for these Scenarios are shown in Table 1, where a is the semi-major axis, e is the eccentricity, i is the inclination, ω is the argument of periapsis, Ω is the right ascension of the ascending node (RAAN) and ν is the true anomaly.

Table 1: Client and Inspector's Orbital Elements

	a (km)	e	i (°)	Ω (°)	ω (°)	ν (°)
Inspector	7378.1	0.05	4.99976	45	10.0001	45
Client	7378	0.05	5	45	10	45

External perturbations are also considered, which are assumed small, but time varying. The external perterbations are modeled as

$$^{L}\mathbf{F}_d = 0.05 \times \begin{bmatrix} 0.5 - 0.2\sin(0.05t) + 0.8\cos(0.05t) \\ 0.8 + 0.9\sin(0.05t) + 0.5\cos(0.05t) \\ 0.7 + 0.4\sin(0.05t) - 0.6\cos(0.05t) \end{bmatrix} \mathrm{N}. \tag{54}$$

Scenario 1

The first scenario involves a short-range rendezvous maneuver where the inspector is instructed to maneuver to an identified face of a malfunctioning client experiencing an uncontrolled tumble. The desired terminal states are written as

$$\mathbf{x}_d = \begin{bmatrix} 5 \ \mathrm{m} \\ 0 \ \mathrm{rad} \\ 0 \ \mathrm{rad} \end{bmatrix} \text{ and } \quad \dot{\mathbf{x}}_d = \begin{bmatrix} 0 \ \frac{\mathrm{m}}{\mathrm{s}} \\ 0 \ \frac{\mathrm{rad}}{\mathrm{s}} \\ 0 \ \frac{\mathrm{rad}}{\mathrm{s}} \end{bmatrix}. \tag{55}$$

The rendezvous maneuver is propagated for 1 hour, long enough to demonstrate that the desired terminal conditions can be met and maintained. This is shown in Figure 5, where the tracking errors are driven to region around the origin using the proposed ASOFNTSMC. This tracking performance is maintained and chattering effects eliminated despite the inspector's thrusting limitations and the uncertain tumbling nature of the client. The performance of the proposed ASOFNTSMC scheme is tuned using the control parameters written in Table 4. The chattering elimination behavior is shown through the inspector's control profile in Figure 6, which is initially saturated as the controller works to reduce the system's tracking error and force the system trajectories on to the sliding manifold before being attenuated across the remainder of the Simulation. The complete rendezvous trajectory is shown in Figure 7, which depicts the inspector maneuvering into a proximity orbit about a tumbling client. Figure 8 depicts a proximity view with the red surface of the client indicating the selected face for inspection.

Table 2: Scenario 1 Parameters

Parameter	Value
γ_1	1.667
γ_2	3.667
$\mathbf{K}_1$	$\text{diag}([0.007,\ 0.01,\ 0.009])$
$\mathbf{K}_2$	$\text{diag}([0.7,\ 0.7,\ 0.7])$
$\mathbf{K}_3$	$\text{diag}([0.4,\ 0.4,\ 0.4])$
$\mathbf{K}_4$	$\text{diag}([5,\ 5,\ 5])$
δ	0.1
$\bar{\kappa}_1$	10
$\bar{\kappa}_2$	1×10^{-4}
$\bar{\kappa}_3$	5

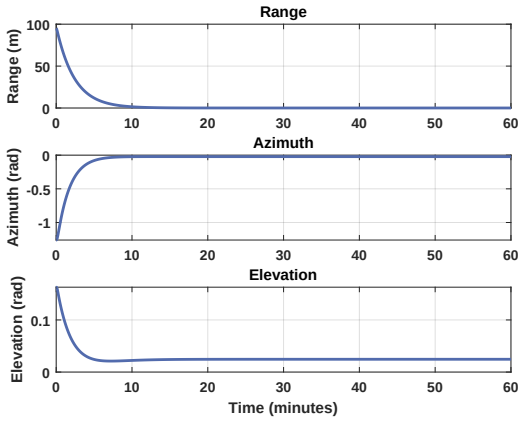

Figure 5: **Inspector's State Errors (Scenario 1)**

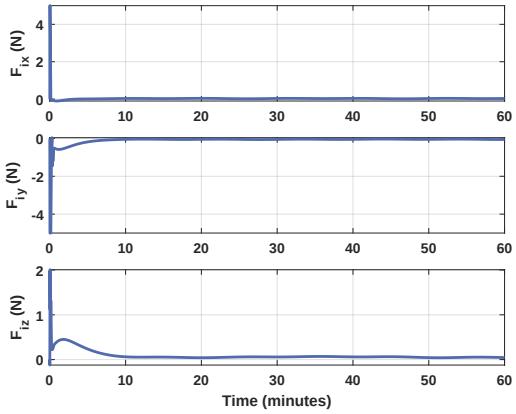

Figure 6: **Inspector's Thrust Profile (Scenario 1)**

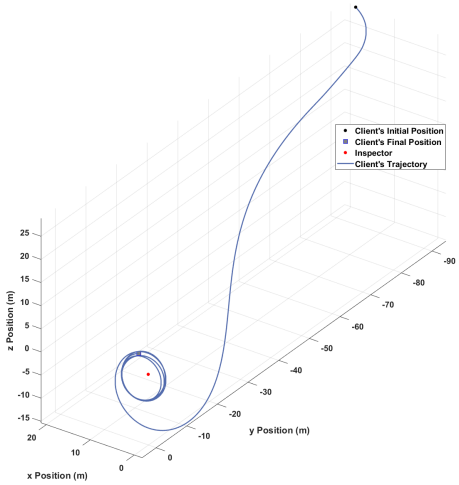

Figure 7: **Inspector's Rendezvous Trajectory (Scenario 1)**

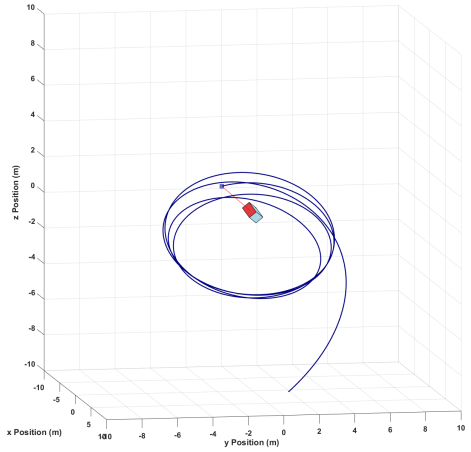

Figure 8: **Inspector's Rendezvous Trajectory - Proximity View (Scenario 1)**

Scenario 2

The next scenario assumes the malfunctioning client is no longer stationary as it tumbles uncontrollably relative to the inspection vehicle, meaning that client can now produce small translational maneuvers, relative to an inspector, in addition to an uncontrolled tumble. The desired terminal states are written as

$$\mathbf{x}_d = \begin{bmatrix} 20 \text{ m} \\ 0 \text{ rad} \\ 0 \text{ rad} \end{bmatrix} \text{ and } \quad \dot{\mathbf{x}}_d = \begin{bmatrix} 0 \ \frac{\text{m}}{\text{s}} \\ 0 \ \frac{\text{rad}}{\text{s}} \\ 0 \ \frac{\text{rad}}{\text{s}} \end{bmatrix}. \tag{56}$$

The control parameters used for this scenario are written as

Table 3: Scenario 2 Parameters

Parameter	Value
γ_1	1.667
γ_2	3.667
$\mathbf{K}_1$	$\text{diag}([0.005,\ 0.009,\ 0.009])$
$\mathbf{K}_2$	$\text{diag}([0.5,\ 0.8,\ 0.8])$
$\mathbf{K}_3$	$\text{diag}([0.3,\ 0.4,\ 0.4])$
$\mathbf{K}_4$	$\text{diag}([3,\ 3,\ 3])$
δ	0.1
$\bar{\kappa}_1$	25
$\bar{\kappa}_2$	4×10^{-3}
$\bar{\kappa}_3$	7

For this scenario, the unknown client maneuver is described as

$${}^{I}\mathbf{F}_c = \begin{bmatrix} 1 \sin(0.005t) \\ 1.5 \sin(0.005t) \\ 2 \sin(0.005t) \end{bmatrix} \text{N}. \tag{57}$$

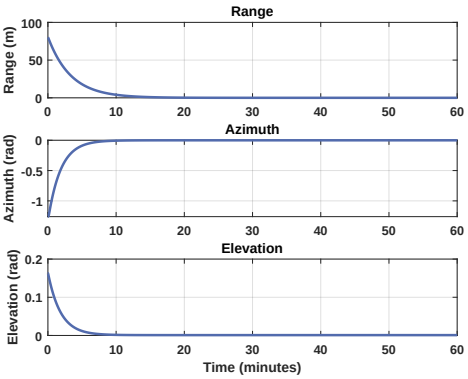

Figure 9: **Inspector's State Errors (Scenario 2)**

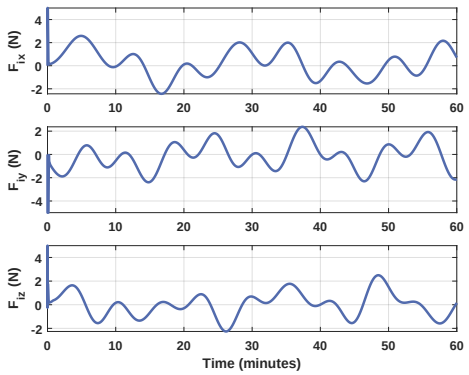

Figure 10: **Inspector's Thrust Profile (Scenario 2)**

The rendezvous simulation is again propagated for 1 hour with the error state trajectories and the inspector's thrust profile being shown in Figure 9 and Figure 10 respectively. The inspector's simulated rendezvous trajectory is shown in Figure 11, with the proximity view depicted in Figure 12. Despite the unknown and

malfunctioning nature of the client, including both tumbling and uncertain maneuvering, as well as external disturbances and the inspector's thrust saturation, the proposed ASOFNTSMC law quickly converges the error states to a region around the origin. It is also observed that the imposed adaptive laws help ensure the inspector's thrusting remains both tractable and reasonable, despite any uncertainties in the client's thrusting capabilities. The trajectory of the inspector-client formation is shown in Figure 13, depicted in the ECI frame.

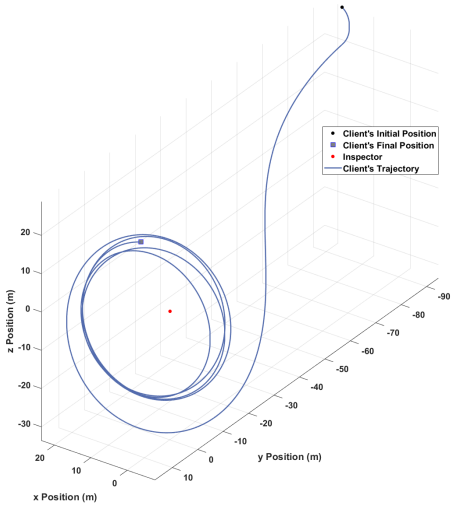

Figure 11: **Inspector's Rendezvous Trajectory (Scenario 2)**

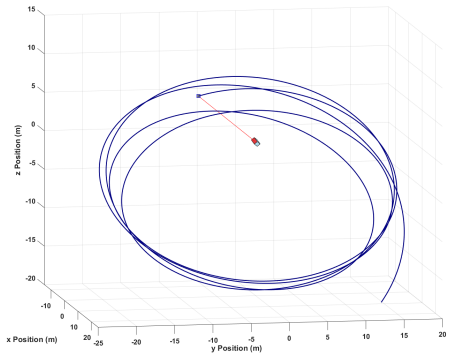

Figure 12: **Inspector's Rendezvous Trajectory - Proximity View (Scenario 2)**

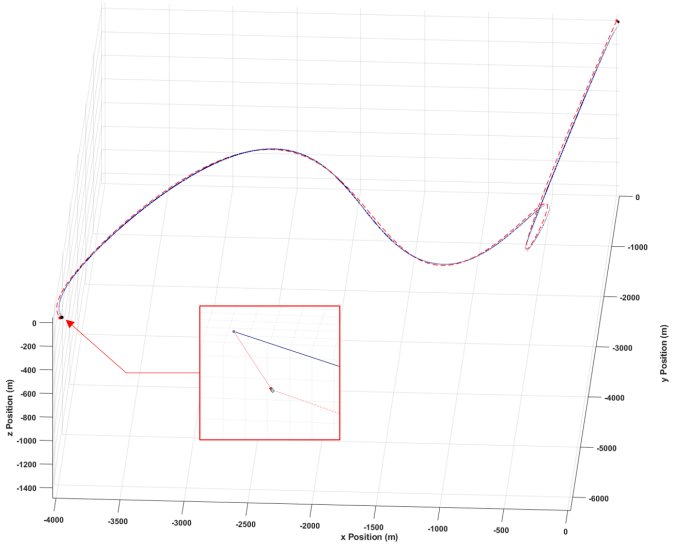

Figure 13: **Inspector's Close Range Proximity Maneuver Within The Client's ECI Frame (Scenario 2)**

Scenario 3

The final scenario assumes a phased approach to a freely tumbling malfunctioning client. The phased approach is defined as

$$\mathbf{x}_{d(T=0)} = \begin{bmatrix} 60 \text{ m} \\ 0 \text{ rad} \\ 0 \text{ rad} \end{bmatrix}, \quad \mathbf{x}_{d(T=1500)} = \begin{bmatrix} 30 \text{ m} \\ 0 \text{ rad} \\ 0 \text{ rad} \end{bmatrix} \quad \mathbf{x}_{d(T=4000)} = \begin{bmatrix} 10 \text{ m} \\ 0 \text{ rad} \\ 0 \text{ rad} \end{bmatrix} \tag{58}$$

and

$$\dot{\mathbf{x}}_{d(T=0)} = \begin{bmatrix} 0 \frac{\text{m}}{\text{s}} \\ 0 \frac{\text{rad}}{\text{s}} \\ 0 \frac{\text{rad}}{\text{s}} \end{bmatrix}, \quad \dot{\mathbf{x}}_{d(T=1500)} = \begin{bmatrix} 0 \frac{\text{m}}{\text{s}} \\ 0 \frac{\text{rad}}{\text{s}} \\ 0 \frac{\text{rad}}{\text{s}} \end{bmatrix} \quad \dot{\mathbf{x}}_{d(T=4000)} = \begin{bmatrix} 0 \frac{\text{m}}{\text{s}} \\ 0 \frac{\text{rad}}{\text{s}} \\ 0 \frac{\text{rad}}{\text{s}} \end{bmatrix}. \tag{59}$$

For this final scenario the client spacecraft's initial angular rate and initial attitude quaternion are defined as

$$\boldsymbol{\omega}_c(0) = \begin{bmatrix} 0.0 & 0.0 & 0.145 \end{bmatrix}^T \tag{60}$$

and

$$\mathbf{q}_c(0) = \begin{bmatrix} 0 & -0.253 & 0 \end{bmatrix}^T \quad \mathbf{q}_{c0}(0) = \sqrt{1 - \mathbf{q}_c'(0)\mathbf{q}_c(0)} \tag{61}$$

respectively, with the control parameters used for this scenario written as

Table 4: Scenario 3 Parameters

Parameter	Value
γ_1	1.667
γ_2	3.667
$\mathbf{K}_1$	$\text{diag}([0.005,\ 0.01,\ 0.07])$
$\mathbf{K}_2$	$\text{diag}([0.7,\ 0.9,\ 0.9])$
$\mathbf{K}_3$	$\text{diag}([0.4,\ 0.7,\ 0.7])$
$\mathbf{K}_4$	$\text{diag}([10,\ 10,\ 10])$
δ	0.1
$\bar{\kappa}_1$	0.1
$\bar{\kappa}_2$	1×10^{-4}
$\bar{\kappa}_3$	5

The rendezvous simulation is propagated for 2.5 hours with the error state trajectories and the inspector's thrust profile being shown in Figure 14 and Figure 15 respectively. The simulated rendezvous trajectory is shown in Figure 16, with the proximity view depicted in Figure 17.

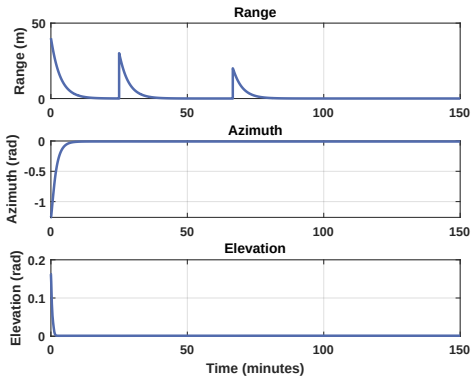

Figure 14: **Inspector's State Errors (Scenario 3)**

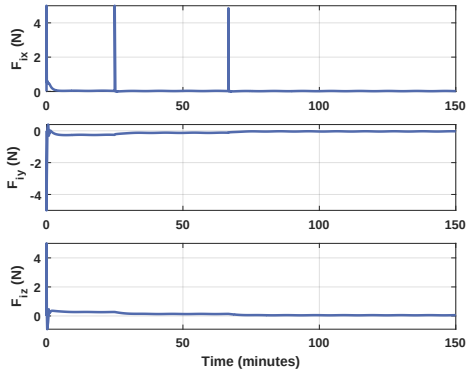

Figure 15: **Inspector's Thrust Profile (Scenario 3)**

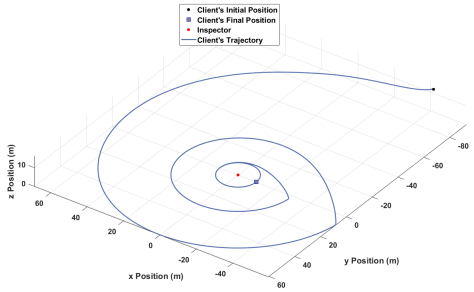

Figure 16: **Inspector's Rendezvous Trajectory (Scenario 3)**

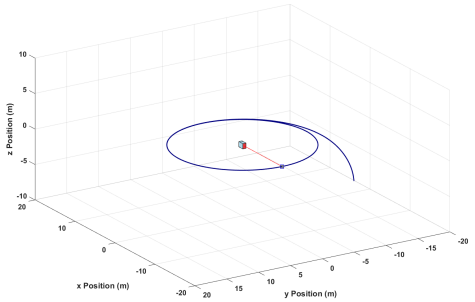

Figure 17: **Inspector's Rendezvous Trajectory - Proximity View (Scenario 3)**

CONCLUSION

This analysis applied a new adaptive second-order fast non-singular terminal sliding mode control scheme to the problem of satellite relative motion. When used in tandem with a LOS-based relative motion model and adequately designed adaptive framework, the suggested control scheme enables an inspection vehicle to approach an uncontrolled client vehicle. This approach was applied to several different scenarios which simulated tumbling and maneuvering aspects of a prospective client, demonstrating the application of the proposed approach to orbital rendezvous sorties with malfunctioning, inoperable, or out of control client vehicles. The suggested control scheme achieved high precession and finite-time reachability to the real sliding mode despite the malfunctioning nature of the client vehicle; steps were taken to alleviate adverse chattering effects to improve control performance.

REFERENCES

[1] Z. Jing, R. Pan, Y. Li, and P. Dong, *Non-Cooperative Target Tracking, Fusion and Control*. Aug. 2018, 10.1007/978-3-319-90716-1.

[2] C. G. Henshaw, S. Glassner, B. Naasz, and B. Roberts, "Grappling Spacecraft," *Annual Review of Control, Robotics, and Autonomous Systems*, Vol. 5, No. 1, 2022, pp. 137–159. _eprint: https://doi.org/10.1146/annurev-control-042920-011106, 10.1146/annurev-control-042920-011106.

[3] B. Barbee, J. Carpenter, S. Heatwole, L. Markley, M. Moreau, B. Naasz, and J. Eepoel, "A Guidance and Navigation Strategy for Rendezvous and Proximity Operations with a Noncooperative Spacecraft in Geosynchronous Orbit," *The Journal of the Astronautical Sciences*, Vol. 58, July 2011, 10.1007/BF03321176.

[4] B. P. Hoskins, "Applications of Adaptive Terminal Sliding Mode Control to Rendezvous with Malfunctioning Clients," *2023 IEEE Aerospace Conference*, 2023.

[5] B. P. Hoskins, "Applications of Adaptive Non-Singular Terminal Sliding Mode Control to Rendezvous with Malfunctioning Clients with Unknown Maneuvers," *46th Annual AAS Guidance, Navigation and Control Conference*, 2023.

[6] B. Tapley, B. Schutz, and G. H. Born, *Statistical Orbit Determination*. Elsevier, June 2004. Google-Books-ID: Ct3qN1VCHewC.

[7] N. R. Boone and R. A. Bettinger, "Artificial Debris Collision Risk Following a Catastrophic Spacecraft Mishap in Lunar Orbit," 2021.

[8] W. Cai, X. H. Liao, and Y. D. Song, "Indirect Robust Adaptive Fault -Tolerant Control for Attitude Tracking of Spacecraft," *Journal of Guidance, Control, and Dynamics*, Vol. 31, Sept. 2008, pp. 1456–1463, 10.2514/1.31158.

[9] Y. Hong, J. Huang, and Y. Xu, "On an output feedback finite-time stabilization problem," *IEEE Transactions on Automatic Control*, Vol. 46, Feb. 2001, pp. 305–309. Conference Name: IEEE Transactions on Automatic Control, 10.1109/9.905699.

[10] S. Yu, X. Yu, B. Shirinzadeh, and Z. Man, "Continuous finite-time control for robotic manipulators with terminal sliding mode," *Automatica*, Vol. 41, Nov. 2005, pp. 1957–1964, 10.1016/j.automatica.2005.07.001.

[11] H. K. Khalil, "Nonlinear systems third edition," *Patience Hall*, Vol. 115, 2002.

[12] R. Ji, D. Li, and J. Ma, "Adaptive Second-Order Fast Nonsingular Terminal Sliding Mode Control for a Tilting Quadcopter," *2022 13th Asian Control Conference (ASCC)*, May 2022, pp. 403–408. ISSN: 2770-8373, 10.23919/ASCC56756.2022.9828145.

[13] W. Gao and J. Hung, "Variable structure control of nonlinear systems: a new approach," *IEEE Transactions on Industrial Electronics*, Vol. 40, Feb. 1993, pp. 45–55. Conference Name: IEEE Transactions on Industrial Electronics, 10.1109/41.184820.

[14] L. Qiao and W. Zhang, "Adaptive Second-Order Fast Nonsingular Terminal Sliding Mode Tracking Control for Fully Actuated Autonomous Underwater Vehicles," *IEEE Journal of Oceanic Engineering*, Vol. 44, Apr. 2019, pp. 363–385. Conference Name: IEEE Journal of Oceanic Engineering, 10.1109/JOE.2018.2809018.

[15] J. Zhou and J. Yang, "Smooth Sliding Mode Control for Missile Interception with Finite-Time Convergence," *Journal of Guidance, Control, and Dynamics*, Vol. 38, July 2015, pp. 1311–1318, 10.2514/1.G000912.

[16] S. Mondal and C. Mahanta, "Adaptive second order terminal sliding mode controller for robotic manipulators," *Journal of the Franklin Institute*, Vol. 351, Apr. 2014, pp. 2356–2377, 10.1016/j.jfranklin.2013.08.027.

[17] H. Du, L. Wang, J. Chen, H. Huang, and X. Feng, "Integral Sliding-Mode Tracking Control for Heavy Vehicle Electrohydraulic Power Steering System," *IEEE/ASME Transactions on Mechatronics*, Vol. 26, June 2021, pp. 1455–1466. Conference Name: IEEE/ASME Transactions on Mechatronics, 10.1109/TMECH.2020.3020956.